

FISTAPruner: Layer-wise Post-training Pruning for Large Language Models

Pengxiang Zhao^{1*} Hanyu Hu^{1*}
Ping Li² Yi Zheng² Zhefeng Wang² Xiaoming Yuan^{1†}

¹ Department of Mathematics, The University of Hong Kong
² System AI Innovation Lab, Huawei Cloud

Abstract

Pruning is a critical strategy for compressing trained large language models (LLMs), aiming at substantial memory conservation and computational acceleration without compromising performance. However, existing pruning methods typically necessitate inefficient retraining for billion-scale LLMs or rely on heuristically designed metrics to determine pruning masks, leading to performance degradation. This paper presents, for the first time, a LASSO-like convex optimization model crafted to induce sparsity in LLMs. By leveraging FISTA, we introduce FISTAPruner, a novel method that includes a cumulative error elimination mechanism within decoder layers and supports parallel pruning for unstructured pruning. Additionally, we extend this method to 2:4 semi-structured pruning. We comprehensively evaluate FISTAPruner on models such as OPT, LLaMA, and Qwen variants with 125M to 70B parameters under unstructured and 2:4 semi-structured sparsity, showcasing superior performance over existing methods across various language benchmarks. Notably, it can remove 50% of the model parameters for LLaMA-3-70B while retaining 98.6% and 95.6% of the zero-shot task performance under these two sparsity patterns, respectively.

1 Introduction

In recent years, large language models (LLMs) have revolutionized the field of natural language processing, achieving impressive results in tasks such as machine translation, sentiment analysis, question answering, and text generation (Lyu et al., 2023; Yao et al., 2023; Zhang et al., 2023a,b; Wang et al., 2023; Arefeen et al., 2024; Li et al., 2024). Advanced LLMs such as OpenAI’s GPT-4 (OpenAI, 2023), Meta’s LLaMA-3 (Meta AI, 2023), and

Google’s Gemini (Gemini Team et al., 2023) excel in generating coherent text with extensive parameters. However, the growth in model sizes outpaces hardware improvements, posing significant deployment and inference challenges (Steiner et al., 2023). For example, operating OPT-175B (Zhang et al., 2022) requires over 320 GB of memory and at least five 80 GB A100 GPUs for loading its parameters in FP16 precision. This challenge becomes more pronounced in environments with limited resources, such as mobile devices, edge computing systems, and real-time applications. Consequently, there has been considerable interest in compressing LLMs to enhance their efficiency and practicality for deployment across various applications.

Pruning is a key method for compressing LLMs, aiming to eliminate redundant weights to reduce model size and computational demands while striving to maintain performance. Methods such as those in (Huang et al., 2020; Ma et al., 2023; Zhang et al., 2023c) require a retraining phase post-pruning, which is inefficient for billion-scale LLMs. PERP (Zimmer et al., 2023) introduces an efficient retraining approach after pruning to recover the performance of the pruned model. Recent developments, including SparseGPT (Frantar and Alistarh, 2023) and Wanda (Sun et al., 2023), employ post-training pruning techniques for LLMs without retraining. These methods, however, rely on the heuristic-based Optimal Brain Surgeon (OBS) framework (Hassibi and Stork, 1992) or utilize heuristic-based pruning metrics to determine pruning masks, potentially compromising performance. DSnoT (Zhang et al., 2023d) introduces a training-free fine-tuning approach that updates the results of other pruning methods, such as SparseGPT and Wanda, which also depend on heuristic-based adjustment metrics.

In this work, we first introduce a LASSO-like convex optimization model for layer-wise post-training unstructured pruning of LLMs (the nov-

*Equal contribution. This work was conducted during an internship at Huawei Cloud.

†Corresponding author: xmyuan@hku.hk.

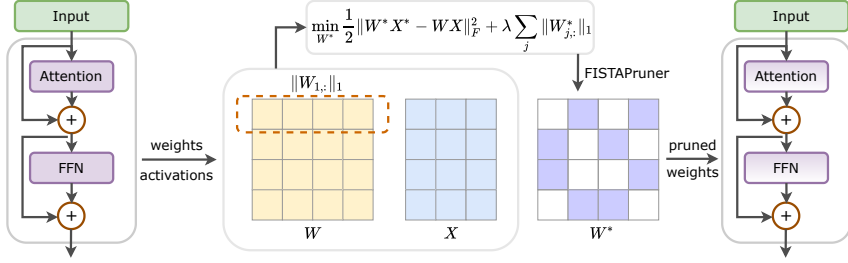


Figure 1: Overview of the proposed FISTAPruner. Given a weight matrix \mathbf{W} and its corresponding input feature activation \mathbf{X} , we employ the proposed convex optimization model, utilizing FISTA, to derive the pruned weights.

elty compared to traditional LASSO-based pruning methods is detailed in Appendix C). Figure 1 provides an overview of our method, which is applied to each linear operator. We employ the Frobenius norm of the difference between the outputs obtained from the dense and pruned weights to quantify the output error. Additionally, we integrate an ℓ_1 -norm regularization term, the optimal convex approximation of the ℓ_0 -norm (Candès et al., 2006), into each row of weights to promote sparsity. The solutions of the proposed optimization model demonstrate a balanced trade-off between output error and sparsity, governed by our proposed adaptive tuning method that meticulously adjusts the hyperparameter λ . To solve this optimization problem efficiently, we utilize the Fast Iterative Shrinkage-Thresholding Algorithm (FISTA) (Beck and Teboulle, 2009), which ensures a convergence rate of $O(1/k^2)$. Following this, we name our proposed method FISTAPruner. We further extend it to accommodate 2:4 semi-structured pruning by incorporating a hard thresholding step following FISTA’s convergence, thus achieving the desired sparsity structures.

In addition, our approach effectively mitigates the cumulative error within decoder layers resulting from pruning by incorporating an intra-layer error correction mechanism. Due to discrepancies between the outputs of dense and pruned weights, errors can accumulate, as the output from one pruned operator becomes the input for the next. FISTAPruner addresses this by sequentially pruning the weights of each linear operator within a decoder layer, using the output from the pruned weights of one operator as the input for the next, thus minimizing output discrepancies. Additionally, FISTAPruner treats each decoder layer as an independent unit for pruning, allowing for the simultaneous pruning of multiple decoder layers and significantly increases efficiency.

We empirically evaluate FISTAPruner on the widely adopted OPT (Zhang et al., 2022), LLaMA (Touvron et al., 2023a), LLaMA-2 (Touvron et al., 2023b), LLaMA-3 (Touvron et al., 2023a), and Qwen2.5 (Qwen Team, 2025) model families. FISTAPruner’s layer-by-layer pruning implementation allows for the pruning of these LLMs ranging from 125M to 70B parameters on a single NVIDIA A100 GPU with 40 GB of memory. Our results confirm that FISTAPruner can efficiently create sparse networks from pretrained LLMs without retraining. Moreover, our approach surpasses the performance of baseline methods such as SparseGPT, Wanda, DSnoT, and PERP across various language benchmarks. We also perform a series of ablation studies to validate our methods. We believe our work sets a new direction and baseline for future research in this area and encourages further exploration into understanding sparsity in LLMs with the tools of convex optimization.

2 Background and Related Work

Pruning of LLMs. Pruning is a widely used strategy to compress LLMs by generating sparse weight matrices under unstructured, semi-structured, and structured sparsity based on calibration data. Unstructured sparsity of rate $s\%$, eliminates $s\%$ of the entries in a weight matrix. Semi-structured sparsity with proportion $n : m$ maintains a fixed overall sparsity level n/m , and allows at most n non-zero entries in every group of m consecutive entries. Pruning weights into semi-structured sparsity, especially with proportion 2:4, can yield up to 2 \times inference speedup using NVIDIA GPUs with the Ampere architecture (Mishra et al., 2021) and hence is of particular interest. Structured sparsity, which zeroes entire rows or columns, offers significant computational and memory benefits but can lead to greater performance losses.

Pruning with Retraining. Traditional pruning pipelines often include a retraining step to offset performance losses (Huang et al., 2020; Ma et al., 2023; Zhang et al., 2023c). However, the sheer scale of LLMs makes this additional retraining costly in both time and computational resources. (Dinh et al., 2020; Holmes et al., 2021; Xie et al., 2023) integrate retraining directly into the pruning process by targeting the minimization of the highly non-convex loss function related to the calibration dataset, using the alternating direction method of multipliers (ADMM) to derive pruned weights. Nonetheless, this approach imposes significant computational demands and the use of ADMM in non-convex optimization often results in unstable performance (He and Yuan, 2012).

Pruning without Retraining. Pruning without retraining offers a straightforward alternative, eliminating the need for post-pruning retraining. These methods prune LLMs in a single step, simplifying implementation and reducing both time and computational demands. Consequently, various methods have been developed under different sparsity frameworks. For structured pruning, SliceGPT (Ashkboos et al., 2024) utilizes principal component analysis to prune rows and columns of weights to reduce model dimensions. ZipLM (Kurtić et al., 2024) adopts an OBS-based approach for structured pruning and updates remaining weights to maintain performance. Our proposed FISTAPruner focuses on unstructured and semi-structured pruning, and thus is orthogonal to these structured pruning methods, enabling further model compression. For unstructured and semi-structured pruning, SparseGPT (Frantar and Alistarh, 2023) and ISC (Shao et al., 2024) leverage the OBS framework to calculate saliency for each entry using the inverse Hessian of the loss metric, based on which pruning masks are generated and weights are updated. Wanda (Sun et al., 2023) implements a heuristic approach, removing weights based on the product of their magnitudes and activations without compensation. DSnoT (Zhang et al., 2023d) updates the results of other pruning methods, such as SparseGPT and Wanda, which also relies on heuristic-based adjustment metrics. (Boža, 2024) employs ADMM to optimize weight updates under iteratively refined pruning masks chosen through heuristic methods based on Wanda. These methods adopt a layer-wise pruning strategy, where errors between the pruned output and the original output of each operator accumulate. Moreover, due

to their heuristic nature, the performances of the pruned models are unstable and compromised.

Error Corrections. Error correction techniques are increasingly used to mitigate error accumulation from layer-wise pruning by minimizing reconstruction errors between the pruned network and the original one (Park et al., 2024; El Halabi et al., 2022). However, their implementations and applications to pruning LLMs vary widely. Prominent methods like SparseGPT (Frantar and Alistarh, 2023) focus on pruning without explicit error correction, while approaches like K-prune (Park et al., 2024) minimize global reconstruction error, facing scalability challenges as globally correcting pruning errors requires global sequential pruning. Our work introduces intra-layer error corrections for better accuracy and computational efficiency. By focusing on intra-layer adjustments, our method provides a scalable and effective solution for pruning LLMs.

3 Methodology

In this section, we introduce our post-training pruning method, FISTAPruner, which comprises three main components. First, we address the error accumulation issue in layer-wise pruning with an intra-layer error correction mechanism and develop a novel convex optimization model tailored for this purpose. We then detail the process for unstructured pruning using FISTA and adapt the framework for $n : m$ semi-structured pruning. Finally, we present an adaptive method that finely tunes the hyperparameter λ in our model to minimize the output discrepancies between dense and pruned operators while achieving the desired sparsity level.

3.1 Post-Training Pruning Model

Post-training compression is typically achieved by decomposing the full-model compression problem into layer-wise subproblems (Frantar and Alistarh, 2023). For instance, a typical Transformer decoder layer (Vaswani et al., 2017) comprises six crucial linear operators: W_Q , W_K , W_V , W_O , W_{fc_1} , and W_{fc_2} . We leverage an intra-layer error correction mechanism that sequentially prunes the weights while explicitly accounting for the cumulative error introduced at each step. Consider a dense weight matrix $\mathbf{W} \in \mathbb{R}^{m \times n}$ and the corresponding input activation $\mathbf{X} \in \mathbb{R}^{n \times p}$. The output is $\mathbf{Z} = \mathbf{W}\mathbf{X}$. Our goal is to find the pruned weights \mathbf{W}^* that minimize the discrepancy between the outputs of

the dense and pruned models:

$$\min_{\mathbf{W}^*} \|\mathbf{W}^* \mathbf{X}^* - \mathbf{W} \mathbf{X}\|_F^2 \quad \text{s.t.} \quad \mathbf{W}^* \in \mathcal{S}, \quad (1)$$

where $\|\cdot\|_F$ denotes the Frobenius norm, and \mathcal{S} defines the permissible sparsity patterns. The input activation \mathbf{X}^* is defined based on the position of the operator within the layer. Specifically, if the operator is at the top of the layer, then $\mathbf{X}^* = \mathbf{X}$. Conversely, if the operator follows previously pruned operators, \mathbf{X}^* is set to $\mathbf{Z}_{\text{prev}}^*$, where $\mathbf{Z}_{\text{prev}}^*$ is the pruned output from the preceding operator.

As illustrated in Figure 2, consider two sequential operators with weights \mathbf{W}_1 and \mathbf{W}_2 . When pruning \mathbf{W}_1 to obtain its pruned counterpart \mathbf{W}_1^* , Equation 1 quantifies the output error between $\mathbf{W}_1 \mathbf{X}$ and $\mathbf{W}_1^* \mathbf{X}$, where the input \mathbf{X}^* remains the same as \mathbf{X} since this operator is at the top of the layer. However, for the second operator \mathbf{W}_2^* , the corresponding input becomes $\mathbf{W}_1^* \mathbf{X}$ instead of $\mathbf{W}_1 \mathbf{X}$ due to the pruning applied to \mathbf{W}_1 . Consequently, the deviation between the outputs of \mathbf{W}_2 and \mathbf{W}_2^* is computed by comparing $\mathbf{W}_2(\mathbf{W}_1 \mathbf{X})$ and $\mathbf{W}_2^*(\mathbf{W}_1^* \mathbf{X})$. This approach ensures that cumulative error is appropriately considered, as each pruning step accounts for both the changes in the weights and the modified input activations resulting from previous pruning. Note that we use intra-layer error corrections within each decoder layer, enabling parallel pruning and improved performance (see Section F.1 for details).

Unstructured pruning essentially transforms dense weight matrices into sparse structures. The ℓ_0 -norm, which directly counts the number of non-zero entries in a vector, is the most straightforward measure of unstructured sparsity. Despite the intuitive appeal of the ℓ_0 -norm, it induces non-convex and NP-hard optimization challenges. As a result, we adopt the ℓ_1 -norm, its tightest convex relaxation (Candès et al., 2006), to achieve similar sparsity with tractable computational demands. Specifically, we apply the ℓ_1 -norm to each row of \mathbf{W}^* , thereby promoting sparsity throughout the matrix (see Appendix A for detailed explanations):

$$\|\mathbf{W}_{i,:}^*\|_1, \quad i = 1, 2, \dots, m, \quad (2)$$

where $\mathbf{W}_{i,:}^*$ represents the i -th row of \mathbf{W}^* . Then, we construct our optimization model by integrating Equation 1 and Equation 2:

$$\min_{\mathbf{W}^*} \frac{1}{2} \|\mathbf{W}^* \mathbf{X}^* - \mathbf{W} \mathbf{X}\|_F^2 + \lambda \sum_{i=1}^m \|\mathbf{W}_{i,:}^*\|_1. \quad (3)$$

This model aims to simultaneously minimize both the output error and the sum of the ℓ_1 -norm values while the hyperparameter $\lambda > 0$ balances these two terms.

Remark 1. *The proposed optimization model in Equation 3 is convex. This is due to the fact that the square of the Frobenius norm is a convex function, as is the ℓ_1 -norm. Thus, the objective function, being a sum of these two convex functions, is also convex. Since the problem is an unconstrained optimization with a convex objective function, the overall optimization model is convex.*

3.2 Optimization based on FISTA

To deal with the non-smooth regularization term in Equation 3, a straightforward approach is to use subgradient descent methods (Beck, 2017). However, its slow convergence rate of $\mathcal{O}(1/\sqrt{k})$ is not desirable. We thus turn to FISTA (Beck and Teboulle, 2009) with convergence rate $\mathcal{O}(1/k^2)$ to solve the proposed model Equation 3 efficiently. Specifically, starting with $t_0 = 1$ and an initial \mathbf{W}_0^* , the k -th iteration of FISTA reads:

$$\mathbf{W}_{k+1}^* = \mathbf{W}_k^* - \frac{1}{L} (\mathbf{W}_k^* \mathbf{X}(\mathbf{X}^*)^\top - \mathbf{W} \mathbf{X}(\mathbf{X}^*)^\top), \quad (4a)$$

$$\mathbf{W}_{k+2}^* = \text{SoftShrinkage}_{\frac{\lambda}{L}}(\mathbf{W}_{k+1}^*), \quad (4b)$$

$$t_{k+1} = \frac{1}{2} \left(1 + \sqrt{1 + 4t_k^2} \right), \quad (4c)$$

$$\mathbf{W}_{k+1}^* = \mathbf{W}_{k+2}^* + \frac{t_k - 1}{t_{k+1}} (\mathbf{W}_{k+2}^* - \mathbf{W}_k^*), \quad (4d)$$

where $L = \|\mathbf{X}^*(\mathbf{X}^*)^\top\|_2$ is the maximum eigenvalue of $\mathbf{X}^*(\mathbf{X}^*)^\top$ and the SoftShrinkage $_{\rho}(\cdot)$ operator with parameter $\rho \geq 0$ on a matrix $\mathbf{X} = (x_{ij}) \in \mathbb{R}^{m \times n}$ performs elementwise transformations defined by

$$\text{SoftShrinkage}_{\rho}(\mathbf{X}) = \mathbf{X}',$$

where

$$x'_{ij} = \begin{cases} x_{ij} - \rho, & \text{if } x_{ij} > \rho, \\ x_{ij} + \rho, & \text{if } x_{ij} < -\rho, \\ x_{ij}, & \text{otherwise.} \end{cases}$$

Equation 4a executes a gradient descent update on the parameter \mathbf{W}_k^* , aiming to minimize the function $1/2 \|\mathbf{W}_k^* \mathbf{X}^* - \mathbf{W} \mathbf{X}\|_F^2$ with a step size of $1/L$. Equation 4b does a proximal update, which is defined as:

$$\mathbf{W}_{k+2}^* = \arg \min_{\mathbf{W}^*} \left\{ \frac{L}{2} \left\| \mathbf{W}^* - \mathbf{W}_{k+1}^* \right\|_F^2 + \lambda \sum_{i=1}^m \left\| \mathbf{W}_{i,:}^* \right\|_1 \right\}.$$

Equation 4c and Equation 4d calculate a linear combination of the previous two points,

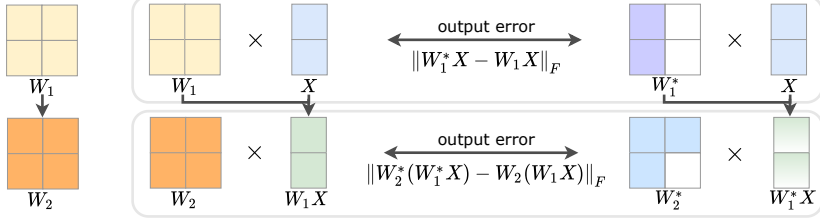


Figure 2: Illustration of the proposed intra-layer error correction mechanism. \mathbf{W}_1 and \mathbf{W}_2 represent the weights of two sequential layers within the network architecture.

$\{\mathbf{W}_{k+2/3}^*, \mathbf{W}_k^*\}$, to facilitate accelerated convergence. Detailed derivations of these steps are provided in Appendix B. The FISTA iteration terminates either when the maximum number of iterations, K , is reached or when the following stopping criterion is satisfied:

$$\|\mathbf{W}_k^* - \mathbf{W}_{k-1}^*\|_F < 1 \times 10^{-6}. \quad (5)$$

3.3 Extension to Semi-structured Pruning

While our convex optimization framework effectively addresses unstructured pruning, practical deployment often necessitates structured or semi-structured sparsity patterns to fully leverage hardware acceleration capabilities. One notable pattern is the 2:4 semi-structured sparsity, which is supported by NVIDIA’s Ampere architecture (Mishra et al., 2021), enabling significant speedups in inference.

The inclusion of the $n : m$ sparsity constraint renders the optimization problem non-convex due to the combinatorial nature of selecting which elements to prune within each group. To tackle this challenge, we adopt FISTA updates, incorporating a hard thresholding step as follows:

$$\mathbf{W}_{K+1}^* = \mathcal{H}(\mathbf{W}_K^*, n : m), \quad (6)$$

where \mathbf{W}_K^* denotes the result from the K -th iteration of FISTA satisfying the stopping criterion, and $\mathcal{H}(\cdot)$ is the hard thresholding, which, for each group of four consecutive elements in every row, sets the two elements with the smallest absolute values to zero and retains the other two.

We acknowledge that the non-convex nature of this extension introduces complexities in theoretical analysis. However, the empirical success observed in our experiments provides confidence in the practical applicability of our approach.

3.4 Adaptive Hyperparameter Tuning

In Equation 3, the regularization parameter λ plays a pivotal role in balancing the trade-off between the

output error and the sparsity of the pruned weights \mathbf{W}^* . A larger λ emphasizes sparsity, potentially increasing the output error, while a smaller λ focuses on minimizing the output error, resulting in less sparsity. To attain a specific desired sparsity level, it is essential to select an appropriate value of λ that guides the optimization toward the target sparsity.

To automate the selection of λ , we propose employing an adaptive hyperparameter tuning mechanism based on the bisection method. This method iteratively adjusts λ within a predefined interval $[0, M]$, where M is a sufficiently large upper bound, to find the optimal value that yields the target sparsity upon solving the optimization problem using FISTA. We establish theoretical guarantees for the convergence of this method in the context of unstructured pruning, as stated in the following theorem:

Theorem 1. *Let $s(\lambda)$ denote the sparsity level (the ratio of zero elements) obtained from ℓ_1 -regularized optimization. Given a target sparsity $s \in (0, 1)$, tolerance $\epsilon > 0$, and initial bounds $\lambda_{\text{low}} < \lambda_{\text{high}}$ satisfying $s(\lambda_{\text{low}}) \leq s \leq s(\lambda_{\text{high}})$, the bisection method terminates after finitely many iterations and returns λ^* such that $|s(\lambda^*) - s| \leq \epsilon$.*

The proof is detailed in Appendix D. Although the adaptive hyperparameter tuning effectively identifies a λ^* that yields a sparsity level close to the desired one, it may not always achieve the exact target due to the inherent continuous nature of the optimization process and limitations in numerical precision. To precisely attain the desired unstructured sparsity, we also implement a final hard thresholding step similar to Equation 6: after obtaining the optimized weights, the smallest-magnitude weights are set to zero until the exact sparsity level is achieved. To adjust λ considering this hard thresholding step, we define the total error

Algorithm 1 FISTAPruner

Inputs: original output $\mathbf{W}\mathbf{X}$, input activation \mathbf{X}^* , \mathbf{W}_0^* , $\lambda, K, T, \epsilon, s\%$ or $n : m$
 $t \leftarrow 0$; $\mathbf{W}_{\text{best}}^* \leftarrow \mathbf{W}_0^*$; $\mathcal{E}_{\text{best}} \leftarrow \|\mathbf{W}_0^* \mathbf{X}^* - \mathbf{W}\mathbf{X}\|_F$
repeat
 $\mathbf{W}_K^* \leftarrow \text{FISTA}(\mathbf{W}\mathbf{X}, \mathbf{X}^*, \lambda, \mathbf{W}_{\text{best}}^*, K)$
 $\mathbf{W}_{K+1}^* \leftarrow \mathcal{H}(\mathbf{W}_K^*, s\% \text{ or } n : m)$
 $\mathcal{E}_{\text{total}} \leftarrow \|\mathbf{W}_{K+1}^* \mathbf{X}^* - \mathbf{W}\mathbf{X}\|_F$
 $\mathcal{E}_{\text{round}} \leftarrow \mathcal{E}_{\text{total}} - \|\mathbf{W}_K^* \mathbf{X}^* - \mathbf{W}\mathbf{X}\|_F$
 if $\mathcal{E}_{\text{total}} < \mathcal{E}_{\text{best}}$ **then**
 $\mathbf{W}_{\text{best}}^* \leftarrow \mathbf{W}_{K+1}^*$
 $\mathcal{E}_{\text{stop}} = (\mathcal{E}_{\text{best}} - \mathcal{E}_{\text{total}}) / \mathcal{E}_{\text{best}}$
 $\mathcal{E}_{\text{best}} \leftarrow \mathcal{E}_{\text{total}}$
 else
 $t \leftarrow t + 1$
 end if
 update λ based on $\mathcal{E}_{\text{round}} / \mathcal{E}_{\text{total}}$ as in Section 3.4
until $t \geq T$ **or** $\mathcal{E}_{\text{stop}} < \epsilon$
return $\mathbf{W}_{\text{best}}^*$

$\mathcal{E}_{\text{total}}$ and the rounding error $\mathcal{E}_{\text{round}}$ as

$$\mathcal{E}_{\text{total}} := \|\mathbf{W}_{K+1}^* \mathbf{X}^* - \mathbf{W}\mathbf{X}\|_F,$$

$$\mathcal{E}_{\text{round}} := \mathcal{E}_{\text{total}} - \|\mathbf{W}_K^* \mathbf{X}^* - \mathbf{W}\mathbf{X}\|_F.$$

A high $\mathcal{E}_{\text{round}} / \mathcal{E}_{\text{total}}$ suggests that the majority of the error originates from the hard thresholding step. This suggests that the sparsity level of \mathbf{W}_K achieved via FISTA falls short of the desired sparsity, implying a need to increase the value of λ to enhance the emphasis on the ℓ_1 -norm in Equation 3. Conversely, a low $\mathcal{E}_{\text{round}} / \mathcal{E}_{\text{total}}$ indicates that the sparsity in \mathbf{W}_K^* is adequate. This observation implies that a reduction in λ might be beneficial. Such an adjustment would shift the model’s emphasis towards minimizing output errors, thereby potentially decreasing the total error. Incorporating the above insights, we apply a threshold ξ for $\mathcal{E}_{\text{round}} / \mathcal{E}_{\text{total}}$.

3.5 FISTAPruner Pseudocode

While the intra-layer error correction mechanism requires sequential pruning of the operators within a decoder layer, we could treat each decoder layer as an independent pruning unit, enabling parallel pruning across multiple decoder layers on different devices, which significantly enhances the efficiency. Within each decoder layer, the proposed FISTAPruner sequentially prunes weights to eliminate error accumulations, as detailed in Section 3.1. Algorithm 1 presents FISTAPruner for the dense weight matrix \mathbf{W} . It leverages FISTA to generate candidate sparse weights based on the model Equation 3, as detailed in Section 3.2. It then applies a hard thresholding step to meet specified sparsity constraints. Additionally, the parameter λ is adap-

tively tuned, as detailed in Section 3.4, to optimize the trade-off between output error and sparsity. The algorithm iteratively updates the weights, preserving the best solution $\mathbf{W}_{\text{best}}^*$, based on the lowest total error $\mathcal{E}_{\text{total}}$. It terminates when the number of consecutive iterations without an improvement in $\mathbf{W}_{\text{best}}^*$ reaches T , or when the improvement ratio $(\mathcal{E}_{\text{best}} - \mathcal{E}_{\text{total}}) / \mathcal{E}_{\text{best}}$ falls below the threshold ϵ .

4 Experiments

In this section, we detail a comprehensive set of experiments designed to validate the efficacy of FISTAPruner. We begin with an in-depth review of our experimental setup. Following this, we explore the perplexity and zero-shot capabilities of the pruned LLMs through rigorous testing and a series of ablation studies. Due to page length constraints, a portion of the results are presented in Appendix E and F.

4.1 Settings

Models. We utilize models from the OPT (Zhang et al., 2022), LLaMA (Touvron et al., 2023a), LLaMA-2 (Touvron et al., 2023b), LLaMA-3 (Meta AI, 2023), and Qwen2.5 (Qwen Team, 2025) families.

Benchmarks. Our primary assessment focuses on evaluating the perplexity of pruned LLMs, a metric renowned for its reliability in assessing LLM performance. Following methodologies from previous studies (Frantar and Alistarh, 2023; Sun et al., 2023), we measure model perplexity using the WikiText-2-raw (Merity et al., 2016) (hereafter shortened to WikiText), PTB (Marcus et al., 1994), and C4 (Raffel et al., 2020) datasets. Additionally, we perform a comprehensive evaluation of the zero-shot capabilities of pruned LLaMA-3-70B models using several standard common-sense benchmark datasets. These include ARC Easy and ARC Challenge (Clark et al., 2018), WinoGrande (Sakaguchi et al., 2021), BoolQ (Clark et al., 2019), RTE (Wang et al., 2018), QNLI (Wang et al., 2018), and WNLI (Wang et al., 2018) tasks, facilitated by the LM Harness library (Gao et al., 2021).

Baselines. We compare FISTAPruner against two widely-used baseline methods: SparseGPT (Frantar and Alistarh, 2023) and Wanda (Sun et al., 2023). Additionally, we evaluate against the latest training-free approach, DSnoT (Zhang et al., 2023d), which updates the results of other pruning methods, and the recent efficient prune-retrain ap-

Table 1: WikiText perplexity (\downarrow) of pruned OPT models under 50% unstructured and 2:4 semi-structured sparsity. FISTAPruner outperforms baseline methods.

OPT								
Method	Sparsity	125M	350M	1.3B	2.7B	6.7B	13B	30B
Dense	0%	27.66	22.00	14.63	12.47	10.86	10.13	9.56
SparseGPT	50%	37.01	31.53	17.55	13.46	11.60	11.15	9.77
Wanda	50%	38.96	36.22	18.41	14.22	11.98	11.93	10.03
FISTAPruner	50%	33.54	28.89	17.21	13.22	11.36	10.95	9.71
SparseGPT	2:4	60.02	50.15	23.83	17.20	14.13	12.94	10.92
Wanda	2:4	80.32	113.00	28.25	21.25	15.90	15.56	13.40
FISTAPruner	2:4	45.16	40.41	22.46	15.70	13.16	12.21	10.54

Table 2: WikiText perplexity (\downarrow) of pruned LLaMA, LLaMA-2, LLaMA-3, and Qwen2.5 models under 50% unstructured and 2:4 semi-structured sparsity. FISTAPruner outperforms baseline methods.

Method	Sparsity	LLaMA				LLaMA-2			LLaMA-3		Qwen2.5	
		7B	13B	30B	65B	7B	13B	70B	8B	70B	0.5B	1.5B
Dense	0%	5.68	5.09	4.10	3.53	5.12	4.57	3.12	5.54	2.59	13.07	9.27
SparseGPT	50%	7.24	6.22	5.33	4.60	6.54	5.63	3.99	8.64	5.30	20.36	13.08
Wanda	50%	7.26	6.15	5.25	4.60	6.46	5.58	3.97	9.06	5.33	25.83	14.11
FISTAPruner	50%	6.97	6.06	5.09	4.39	6.35	5.47	3.93	8.00	5.09	19.61	12.51
SparseGPT	2:4	11.32	9.11	7.21	6.24	10.37	8.29	5.38	14.65	8.63	37.42	21.81
Wanda	2:4	11.54	9.61	6.91	6.24	11.34	8.35	5.20	22.56	8.34	81.59	47.20
FISTAPruner	2:4	9.82	8.27	6.70	5.82	9.63	7.69	5.16	14.54	7.55	33.53	20.14

proach, PERP (Zimmer et al., 2023). We evaluate two types of sparsity configurations: unstructured and 2:4 semi-structured sparsity.

Setup. We implement FISTAPruner using PyTorch (Paszke et al., 2019) and leverage the HuggingFace Transformers library (Wolf et al., 2019) for model and dataset management. All pruning experiments are conducted on NVIDIA A100 GPUs, each equipped with 80 GB of memory. We observe that FISTAPruner efficiently prunes all LLMs using a single GPU and no more than 40 GB of memory. For calibration data, we adhere to the approach outlined in previous works (Frantar and Alistarh, 2023; Sun et al., 2023), utilizing 128 sequences. Each sequence is composed of tokens sampled from the first shard of the C4 dataset, with the number of tokens equal to the maximum embedding length of the LLMs. For parameters of FISTAPruner, we set the initial value of λ to 1×10^{-5} , K to 20, T to 3, M to 10^6 , and ξ to 0.3. For the OPT model family, we use the result of SparseGPT as a warm start for the FISTA iteration and set ϵ to 1×10^{-6} . For the LLaMA model family, we use the result of Wanda as a warm start and set ϵ to 1×10^{-3} .

4.2 Perplexity Experiment Results

In Tables 1 and 2, we present the perplexity results for the pruned OPT, LLaMA, LLaMA-2, LLaMA-3, and Qwen2.5 models of various sizes on Wiki-

Table 3: WikiText perplexity (\downarrow) of pruned LLaMA, LLaMA-2 and LLaMA-3 models under 50% unstructured and 2:4 semi-structured sparsity. FISTAPruner outperforms DSnoT.

Method	Sparsity	7B	13B	30B	2-7B	2-13B	3-8B
Wanda + DSnoT	50%	7.12	6.16	5.20	6.49	5.57	9.07
FISTAPruner	50%	6.97	6.06	5.09	6.35	5.47	8.00
Wanda + DSnoT	2:4	11.54	9.49	7.09	11.53	8.52	20.56
FISTAPruner	2:4	9.82	8.27	6.70	9.63	7.69	14.54

Table 4: WikiText perplexity (\downarrow) of pruned OPT models under 50% sparsity. FISTAPruner outperforms the prune-retrain approach PERP.

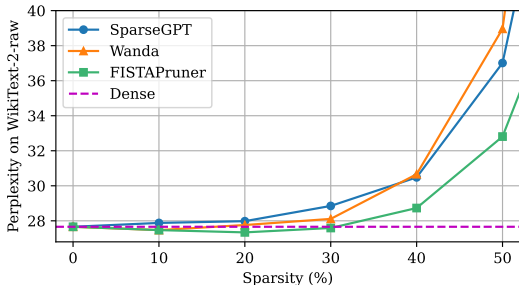
Method	Sparsity	2.7B	6.7B	13B	30B
SparseGPT + PERP	50%	13.40	11.47	10.85	9.76
Wanda + PERP	50%	13.88	11.83	11.06	10.04
FISTAPruner	50%	13.22	11.36	10.95	9.71

Text. For results on PTB and C4, please refer to Appendix E.1 and E.2. We achieved a 50% unstructured or 2:4 semi-structured sparsity level by pruning all linear operators, excluding embeddings and the model head. The data in Tables 1 and 2 illustrate consistent improvements with FISTAPruner over SparseGPT and Wanda.

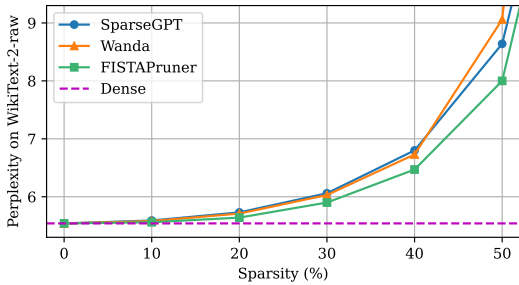
In Tables 3, we detail the comparison between FISTAPruner and DSnoT on LLaMA, LLaMA-2, and LLaMA-3 models of various sizes on WikiText. The data consistently indicate that FISTAPruner

Table 5: Zero-shot results (accuracy, \uparrow) of the pruned LLaMA-3-70B model under 50% unstructured and 2:4 semi-structured sparsity. FISTAPruner outperforms baseline methods on most of the tasks and yields much higher average accuracies especially under 2:4 semi-structured sparsity.

Method	Sparsity	ARC-c	ARC-e	WinoGrande	RTE	BoolQ	QNLI	WNLI	Mean
Dense	0%	0.6024	0.8685	0.8035	0.6859	0.8560	0.5190	0.7183	0.7219
SparseGPT	50%	0.5401	0.8340	0.7979	0.7040	0.8480	0.5035	0.7042	0.7045
Wanda	50%	0.5427	0.8320	0.7814	0.7076	0.8480	0.5045	0.6338	0.6928
FISTAPruner	50%	0.5614	0.8410	0.8035	0.6895	0.8645	0.5055	0.7183	0.7120
SparseGPT	2:4	0.4590	0.7830	0.7609	0.6426	0.8165	0.4985	0.5493	0.6443
Wanda	2:4	0.4829	0.7860	0.7174	0.6354	0.7615	0.5390	0.6056	0.6468
FISTAPruner	2:4	0.4735	0.7985	0.7751	0.7004	0.8540	0.5675	0.6620	0.6901



(a) Perplexity-vs-Sparsity on OPT-125M.



(b) Perplexity-vs-Sparsity on LLaMA-3-8B.

Figure 3: Comparative analysis of sparsity versus perplexity across different methods for OPT-125M and LLaMA-3-8B models on WikiText dataset.

achieves lower perplexity scores, thereby surpassing DSnoT in performance.

We also compare FISTAPruner with the prune-retrain method PERP, with results presented in Table 4. These results demonstrate that FISTAPruner, without any retraining, outperforms the results of SparGPT/Wanda retrained using PERP. Moreover, our method is also compatible with retraining methods and could serve as a superior initialization point in the retraining process.

To further investigate FISTAPruner’s performance under different unstructured sparsity levels, we conducted experiments on the OPT-125M and LLaMA-3-8B models, with perplexity results

visualized in Figure 3 and measured using WikiText. The results indicate that FISTAPruner consistently outperforms existing methods across different levels of unstructured sparsity. Notably, at 20% unstructured sparsity on the OPT-125M model, FISTAPruner’s performance even surpasses that of the dense network.

4.3 Zero-Shot Task Results

The results of zero-shot tasks on pruned LLaMA-3-70B models, with 50% unstructured and 2:4 semi-structured sparsity, are detailed in Table 5. These results indicate that FISTAPruner surpasses existing methods on most tasks. Furthermore, when evaluating the average accuracy across the seven tasks we examined, FISTAPruner consistently shows superior performance compared to existing methods, particularly with 2:4 semi-structured sparsity.

4.4 Ablation Study

We conduct a series of ablation studies to evaluate the impact of the intra-layer error correction mechanism, calibration data, and warm-start mechanism. The results are presented in Appendix F.

5 Conclusion

In this paper, we introduce FISTAPruner, a layer-wise post-training pruning method for LLMs. Initially, we develop a convex optimization model that employs the ℓ_1 -norm to induce unstructured sparsity in the weights, complemented by an intra-layer error correction mechanism to eliminate cumulative errors across operators in the traditional pruning process. Subsequently, we utilize FISTA to efficiently solve the proposed model. Additionally, we extend FISTAPruner to accommodate $n : m$ semi-structured pruning. FISTAPruner supports parallel pruning, which can reduce the total pruning time by utilizing various devices simultaneously. Extensive experiments on the OPT, LLaMA,

LLaMA-2, and LLaMA-3 model families demonstrate FISTAPruner’s superior performance compared to existing methods.

Limitations

Despite the rigorous theoretical foundation and impressive pruning performance of FISTAPruner, the time required for pruning remains a limitation of our method compared to SparseGPT and Wanda. This is primarily due to the iterative nature of FISTA and the process of tuning λ . Pruning time varies with model size; for instance, it takes about 10 minutes for OPT-125M, while LLaMA-3-70B requires approximately 12 hours on a single NVIDIA A100 GPU with 40 GB of memory. However, the parallel-pruning capability of FISTAPruner, which allows for simultaneous pruning of multiple decoder layers across various devices, can mitigate this issue to some extent. Furthermore, as post-training pruning is typically an offline process, time sensitivity may not be a critical factor in real-world applications. In addition, FISTAPruner represents an attempt to integrate convex optimization theory and algorithms into LLM applications, potentially inspiring further advancements in this area.

Beyond computation time, GPU memory consumption is a crucial factor, making FISTAPruner more practical than frameworks like “post-training pruning + fine-tuning” (e.g., “Wanda + LoRA”). For example, loading LLaMA-3-70B in FP16 precision alone requires approximately 140 GB of GPU memory ($70 \text{ billion parameters} \times 2 \text{ bytes}$), necessitating at least four NVIDIA A100 GPUs with 40 GB each. In contrast, FISTAPruner is a layer-wise pruning method that treats each decoder layer independently. This design significantly reduces memory overhead by allowing each decoder layer to be loaded and pruned sequentially on the GPU, then offloaded back to the CPU after pruning. Additionally, it also enables parallel pruning across decoder layers. As a result, for LLaMA-3-70B, using a minimal hardware budget ($4 \times \text{A100 40 GB GPUs}$) for fine-tuning, the total pruning time can be reduced from 12 hours to approximately 3 hours.

Additionally, we would like to note that applying LoRA to fine-tune a pruned model presents several challenges. For weights pruned with unstructured or semi-structured sparsity, directly adding LoRA adapters would break the sparsity pattern. To pre-

serve the sparse structure, a separate LoRA path must be introduced, which increases both the number of parameters and the computational complexity of the model.

Acknowledgments

The work of X. Yuan was supported by the Hong Kong Research Grants Council under the GRF project 17309824.

References

Md Adnan Arefeen, Biplob Debnath, and Srimat Chakradhar. 2024. Leancontext: Cost-efficient domain-specific question answering using llms. *Natural Language Processing Journal*, 7:100065.

Saleh Ashkboos, Maximilian L Croci, Marcelo Gennari do Nascimento, Torsten Hoefer, and James Hensman. 2024. SliceGPT: Compress large language models by deleting rows and columns. *arXiv preprint arXiv:2401.15024*.

Hongxiao Bai and Yun Li. 2023. Structured sparsity in the nvidia ampere architecture and applications in search engines. *NVIDIA Developer Blog*.

Amir Beck. 2017. *First-order methods in optimization*. SIAM.

Amir Beck and Marc Teboulle. 2009. A fast iterative shrinkage-thresholding algorithm for linear inverse problems. *SIAM journal on imaging sciences*, 2(1):183–202.

Vladimír Boža. 2024. Fast and optimal weight update for pruned large language models. *arXiv preprint arXiv:2401.02938*.

Emmanuel J Candès, Justin Romberg, and Terence Tao. 2006. Robust uncertainty principles: Exact signal reconstruction from highly incomplete frequency information. *IEEE Transactions on information theory*, 52(2):489–509.

Christopher Clark, Kenton Lee, Ming-Wei Chang, Tom Kwiatkowski, Michael Collins, and Kristina Toutanova. 2019. BoolQ: Exploring the surprising difficulty of natural yes/no questions. *arXiv preprint arXiv:1905.10044*.

Peter Clark, Isaac Cowhey, Oren Etzioni, Tushar Khot, Ashish Sabharwal, Carissa Schoenick, and Oyvind Tafjord. 2018. Think you have solved question answering? try arc, the ai2 reasoning challenge. *arXiv preprint arXiv:1803.05457*.

Thu Dinh, Bao Wang, Andrea Bertozzi, Stanley Osher, and Jack Xin. 2020. Sparsity meets robustness:

Channel pruning for the feynman-kac formalism principled robust deep neural nets. In *Machine Learning, Optimization, and Data Science: 6th International Conference, LOD 2020, Siena, Italy, July 19–23, 2020, Revised Selected Papers, Part II* 6, pages 362–381. Springer.

Marwa El Halabi, Suraj Srinivas, and Simon Lacoste-Julien. 2022. Data-efficient structured pruning via submodular optimization. *Advances in Neural Information Processing Systems*, 35:36613–36626.

Elias Frantar and Dan Alistarh. 2023. Sparsegpt: Massive language models can be accurately pruned in one-shot. In *International Conference on Machine Learning*, pages 10323–10337. PMLR.

Leo Gao, Jonathan Tow, Stella Biderman, Sid Black, Anthony DiPofi, Charles Foster, Laurence Golding, Jeffrey Hsu, Kyle McDonell, Niklas Muennighoff, et al. 2021. A framework for few-shot language model evaluation. *Version v0. 0.1. Sept*, page 8.

Gemini Team, Rohan Anil, Sebastian Borgeaud, Yonghui Wu, Jean-Baptiste Alayrac, Jiahui Yu, Radu Soricut, Johan Schalkwyk, Andrew M Dai, Anja Hauth, et al. 2023. Gemini: a family of highly capable multimodal models. *arXiv preprint arXiv:2312.11805*.

Babak Hassibi and David Stork. 1992. Second order derivatives for network pruning: Optimal brain surgeon. *Advances in neural information processing systems*, 5.

Bingsheng He and Xiaoming Yuan. 2012. On the $o(1/n)$ convergence rate of the douglas–rachford alternating direction method. *SIAM Journal on Numerical Analysis*, 50(2):700–709.

Yihui He, Xiangyu Zhang, and Jian Sun. 2017. Channel pruning for accelerating very deep neural networks. In *Proceedings of the IEEE international conference on computer vision*, pages 1389–1397.

Connor Holmes, Minjia Zhang, Yuxiong He, and Bo Wu. 2021. Nxtransformer: Semi-structured sparsification for natural language understanding via admm. *Advances in neural information processing systems*, 34:1818–1830.

Zhongzhan Huang, Wenqi Shao, Xinjiang Wang, Liang Lin, and Ping Luo. 2020. Convolution-weight-distribution assumption: Rethinking the criteria of channel pruning. *arXiv preprint arXiv:2004.11627*.

Yixin Ji, Yang Xiang, Juntao Li, Qingrong Xia, Ping Li, Xinyu Duan, Zhefeng Wang, and Min Zhang. 2024. Beware of calibration data for pruning large language models. *arXiv preprint arXiv:2410.17711*.

Eldar Kurtić, Elias Frantar, and Dan Alistarh. 2024. Zi-plm: Inference-aware structured pruning of language models. *Advances in Neural Information Processing Systems*, 36.

Junyi Li, Tianyi Tang, Wayne Xin Zhao, Jian-Yun Nie, and Ji-Rong Wen. 2024. Pre-trained language models for text generation: A survey. *ACM Computing Surveys*, 56(9):1–39.

Chenyang Lyu, Jitao Xu, and Longyue Wang. 2023. New trends in machine translation using large language models: Case examples with chatgpt. *arXiv preprint arXiv:2305.01181*.

Xinyin Ma, Gongfan Fang, and Xinchao Wang. 2023. Llm-pruner: On the structural pruning of large language models. *arXiv preprint arXiv:2305.11627*.

Mitch Marcus, Grace Kim, Mary Ann Marcinkiewicz, Robert MacIntyre, Ann Bies, Mark Ferguson, Karen Katz, and Britta Schasberger. 1994. The penn treebank: Annotating predicate argument structure. In *Human Language Technology: Proceedings of a Workshop held at Plainsboro, New Jersey, March 8–11, 1994*.

Stephen Merity, Caiming Xiong, James Bradbury, and Richard Socher. 2016. Pointer sentinel mixture models. *arXiv preprint arXiv:1609.07843*.

Meta AI. 2023. Llama-3: Meta ai’s latest language model. <https://ai.meta.com/blog/meta-llama-3/>.

Asit Mishra, Jorge Albericio Latorre, Jeff Pool, Darko Stosic, Dusan Stosic, Ganesh Venkatesh, Chong Yu, and Paulius Micikevicius. 2021. Accelerating sparse deep neural networks. *arXiv preprint arXiv:2104.08378*.

OpenAI. 2023. Gpt-4 technical report. *arXiv*, pages 2303–08774.

Seungcheol Park, Hojun Choi, and U Kang. 2024. Accurate retraining-free pruning for pretrained encoder-based language models. In *The Twelfth International Conference on Learning Representations*.

Adam Paszke, Sam Gross, Francisco Massa, Adam Lerer, James Bradbury, Gregory Chanan, Trevor Killeen, Zeming Lin, Natalia Gimelshein, Luca Antiga, et al. 2019. Pytorch: An imperative style, high-performance deep learning library. *Advances in neural information processing systems*, 32.

Qwen Team. 2025. Qwen2.5 technical report. *Preprint, arXiv:2412.15115*.

Colin Raffel, Noam Shazeer, Adam Roberts, Katherine Lee, Sharan Narang, Michael Matena, Yanqi Zhou, Wei Li, and Peter J Liu. 2020. Exploring the limits of transfer learning with a unified text-to-text transformer. *Journal of machine learning research*, 21(140):1–67.

Keisuke Sakaguchi, Ronan Le Bras, Chandra Bhagavatula, and Yejin Choi. 2021. Winogrande: An adversarial winograd schema challenge at scale. *Communications of the ACM*, 64(9):99–106.

Hang Shao, Bei Liu, and Yanmin Qian. 2024. One-shot sensitivity-aware mixed sparsity pruning for large language models. In *ICASSP 2024-2024 IEEE International Conference on Acoustics, Speech and Signal Processing (ICASSP)*, pages 11296–11300. IEEE.

Benoit Steiner, Mostafa Elhoushi, Jacob Kahn, and James Hegarty. 2023. Model: memory optimizations for deep learning. In *International Conference on Machine Learning*, pages 32618–32632. PMLR.

Mingjie Sun, Zhuang Liu, Anna Bair, and J Zico Kolter. 2023. A simple and effective pruning approach for large language models. *arXiv preprint arXiv:2306.11695*.

Robert Tibshirani. 1996. Regression shrinkage and selection via the lasso. *Journal of the Royal Statistical Society Series B: Statistical Methodology*, 58(1):267–288.

Hugo Touvron, Thibaut Lavril, Gautier Izacard, Xavier Martinet, Marie-Anne Lachaux, Timothée Lacroix, Baptiste Rozière, Naman Goyal, Eric Hambo, Faisal Azhar, et al. 2023a. Llama: Open and efficient foundation language models. *arXiv preprint arXiv:2302.13971*.

Hugo Touvron, Louis Martin, Kevin Stone, Peter Albert, Amjad Almahairi, Yasmine Babaei, Nikolay Bashlykov, Soumya Batra, Prajjwal Bhargava, Shruti Bhosale, et al. 2023b. Llama 2: Open foundation and fine-tuned chat models. *arXiv preprint arXiv:2307.09288*.

Ashish Vaswani, Noam Shazeer, Niki Parmar, Jakob Uszkoreit, Llion Jones, Aidan N Gomez, Łukasz Kaiser, and Illia Polosukhin. 2017. Attention is all you need. *Advances in neural information processing systems*, 30.

Alex Wang, Amanpreet Singh, Julian Michael, Felix Hill, Omer Levy, and Samuel R Bowman. 2018. Glue: A multi-task benchmark and analysis platform for natural language understanding. *arXiv preprint arXiv:1804.07461*.

Yubo Wang, Xueguang Ma, and Wenhui Chen. 2023. Augmenting black-box llms with medical textbooks for clinical question answering. *arXiv preprint arXiv:2309.02233*.

Wei Wen, Chunpeng Wu, Yandan Wang, Yiran Chen, and Hai Li. 2016. Learning structured sparsity in deep neural networks. *Advances in neural information processing systems*, 29.

Thomas Wolf, Lysandre Debut, Victor Sanh, Julien Chaumond, Clement Delangue, Anthony Moi, Pieric Cistac, Tim Rault, Rémi Louf, Morgan Funtowicz, et al. 2019. Huggingface’s transformers: State-of-the-art natural language processing. *arXiv preprint arXiv:1910.03771*.

Xiufeng Xie, Riccardo Gherardi, Zhihong Pan, and Stephen Huang. 2023. Hollownerf: Pruning hashgrid-based nerfs with trainable collision mitigation. In *Proceedings of the IEEE/CVF International Conference on Computer Vision*, pages 3480–3490.

Binwei Yao, Ming Jiang, Diyi Yang, and Junjie Hu. 2023. Empowering llm-based machine translation with cultural awareness. *arXiv preprint arXiv:2305.14328*.

Biao Zhang, Barry Haddow, and Alexandra Birch. 2023a. Prompting large language model for machine translation: A case study. In *International Conference on Machine Learning*, pages 41092–41110. PMLR.

Susan Zhang, Stephen Roller, Naman Goyal, Mikel Artetxe, Moya Chen, Shuhui Chen, Christopher Dewan, Mona Diab, Xian Li, Xi Victoria Lin, et al. 2022. Opt: Open pre-trained transformer language models. *arXiv preprint arXiv:2205.01068*.

Wenxuan Zhang, Yue Deng, Bing Liu, Sinno Jialin Pan, and Lidong Bing. 2023b. Sentiment analysis in the era of large language models: A reality check. *arXiv preprint arXiv:2305.15005*.

Yuxin Zhang, Mingbao Lin, Yunshan Zhong, Fei Chao, and Rongrong Ji. 2023c. Lottery jackpots exist in pre-trained models. *IEEE Transactions on Pattern Analysis and Machine Intelligence*.

Yuxin Zhang, Lirui Zhao, Mingbao Lin, Yunyun Sun, Yiwu Yao, Xingjia Han, Jared Tanner, Shiwei Liu, and Rongrong Ji. 2023d. Dynamic sparse no training: Training-free fine-tuning for sparse llms. *arXiv preprint arXiv:2310.08915*.

Max Zimmer, Megi Andoni, Christoph Spiegel, and Sebastian Pokutta. 2023. Perp: Rethinking the prune-retrain paradigm in the era of llms. *arXiv preprint arXiv:2312.15230*.

A Derivations of the Proposed Optimization Model

We present detailed derivations of Equation 3 in the following. Given $\mathbf{X}^* \in \mathbb{R}^{n \times p}$ and $\mathbf{W}\mathbf{X} \in \mathbb{R}^{m \times p}$, we want to find a sparse solution $\mathbf{W}^* \in \mathbb{R}^{m \times n}$ that minimizes the pruning metric

$$\|\mathbf{W}^*\mathbf{X}^* - \mathbf{W}\mathbf{X}\|_F. \quad (7)$$

We observe its similarities to the well-known least absolute shrinkage and selection operator (LASSO) (Tibshirani, 1996) problem and thus transform it into a standard LASSO model, which could be efficiently solved by operator-splitting algorithms such as FISTA. To achieve such a transformation, first, we leverage the following equality to write the decision variable \mathbf{W}^* in its vector form:

$$\begin{aligned} & \|\mathbf{W}^*\mathbf{X}^* - \mathbf{W}\mathbf{X}\|_F^2 \\ &= \|(\mathbf{X}^*)^\top(\mathbf{W}^*)^\top - (\mathbf{W}\mathbf{X})^\top\|_F^2 \\ &= \sum_{i=1}^m \left\| (\mathbf{X}^*)^\top(\mathbf{W}_{i,:}^*)^\top - (\mathbf{W}\mathbf{X})_{i,:}^\top \right\|_2^2 \\ &= \left\| \begin{pmatrix} (\mathbf{X}^*)^\top & & \\ & \ddots & \\ & & (\mathbf{X}^*)^\top \end{pmatrix} \begin{pmatrix} (\mathbf{W}_{1,:}^*)^\top \\ (\mathbf{W}_{2,:}^*)^\top \\ \vdots \\ (\mathbf{W}_{m,:}^*)^\top \end{pmatrix} - \begin{pmatrix} (\mathbf{W}\mathbf{X})_{1,:}^\top \\ (\mathbf{W}\mathbf{X})_{2,:}^\top \\ \vdots \\ (\mathbf{W}\mathbf{X})_{m,:}^\top \end{pmatrix} \right\|_2^2. \end{aligned}$$

Then we can rewrite the square of the pruning metric in its vector form,

$$\|\mathbf{A}\mathbf{x} - \mathbf{b}\|_2^2, \quad (8)$$

where

$$\begin{aligned} \mathbf{A} &= \begin{pmatrix} (\mathbf{X}^*)^\top & & \\ & \ddots & \\ & & (\mathbf{X}^*)^\top \end{pmatrix} \in \mathbb{R}^{pm \times nm}, \\ \mathbf{x} &= \begin{pmatrix} (\mathbf{W}_{1,:}^*)^\top \\ (\mathbf{W}_{2,:}^*)^\top \\ \vdots \\ (\mathbf{W}_{m,:}^*)^\top \end{pmatrix} \in \mathbb{R}^{nm}, \quad \mathbf{b} = \begin{pmatrix} (\mathbf{W}\mathbf{X})_{1,:}^\top \\ (\mathbf{W}\mathbf{X})_{2,:}^\top \\ \vdots \\ (\mathbf{W}\mathbf{X})_{m,:}^\top \end{pmatrix} \in \mathbb{R}^{pm}. \end{aligned}$$

Note that finding a sparse \mathbf{W}^* to minimize Equation 7 is equivalent to finding a sparse \mathbf{x} to minimize Equation 8, which could be modeled by the LASSO formulation

$$\min_{\mathbf{x}} \frac{1}{2} \|\mathbf{A}\mathbf{x} - \mathbf{b}\|_2^2 + \lambda \|\mathbf{x}\|_1.$$

Now, we have

$$\begin{aligned} & \frac{1}{2} \|\mathbf{A}\mathbf{x} - \mathbf{b}\|_2^2 + \lambda \|\mathbf{x}\|_1 \\ &= \frac{1}{2} \|\mathbf{W}^*\mathbf{X}^* - \mathbf{W}\mathbf{X}\|_F^2 + \lambda \left\| \begin{pmatrix} (\mathbf{W}_{1,:}^*)^\top \\ (\mathbf{W}_{2,:}^*)^\top \\ \vdots \\ (\mathbf{W}_{m,:}^*)^\top \end{pmatrix} \right\|_1 \\ &= \frac{1}{2} \|\mathbf{W}^*\mathbf{X}^* - \mathbf{W}\mathbf{X}\|_F^2 + \lambda \sum_{i=1}^m \left\| (\mathbf{W}_{i,:}^*)^\top \right\|_1, \end{aligned}$$

and hence, we obtain the proposed optimization model in Equation 3.

B Derivations of the FISTA Iterations

We derive here the FISTA Iterations for the optimization problem Equation 3 in which one full iteration includes a gradient descent step of the quadratic term $\frac{1}{2} \|\mathbf{W}^*\mathbf{X}^* - \mathbf{W}\mathbf{X}\|_F^2$, a proximal step of the regularization term $\lambda \sum_{i=1}^m \left\| (\mathbf{W}_{i,:}^*)^\top \right\|_1$, and a Nesterov acceleration term that yields an improved convergence rate of $O(1/k^2)$ (Beck and Teboulle, 2009).

Let $f : \mathbb{R}^{m \times n} \rightarrow \mathbb{R}_+$ be a function defined by

$$f(\mathbf{Y}) := \frac{1}{2} \|\mathbf{Y}\mathbf{X}^* - \mathbf{W}\mathbf{X}\|_F^2.$$

The gradient of f at $\mathbf{Y} = \mathbf{W}_k^*$ is computed as

$$\begin{aligned} \nabla f(\mathbf{W}_k^*) &= (\mathbf{W}_k^*\mathbf{X}^* - \mathbf{W}\mathbf{X})(\mathbf{X}^*)^\top \\ &= \mathbf{W}_k^*\mathbf{X}^*(\mathbf{X}^*)^\top - \mathbf{W}\mathbf{X}(\mathbf{X}^*)^\top. \end{aligned}$$

Thus, given optimal step size $1/L$ where L is the maximum eigenvalue of $\mathbf{X}^*(\mathbf{X}^*)^\top$ (Beck and Teboulle, 2009), the gradient descent step Equation 4a of FISTA reads as

$$\mathbf{W}_{k+\frac{1}{3}}^* = \mathbf{W}_k^* - \frac{1}{L} (\mathbf{W}_k^*\mathbf{X}^*(\mathbf{X}^*)^\top - \mathbf{W}\mathbf{X}(\mathbf{X}^*)^\top).$$

In the second step Equation 4b, we do a proximal update with respect to the regularization term by solving

$$\min_{\mathbf{W}^*} \frac{L}{2} \|\mathbf{W}^* - \mathbf{W}_{k+\frac{1}{3}}^*\|_F^2 + \lambda \sum_{i=1}^m \|\mathbf{W}_{i,:}^*\|_1. \quad (9)$$

Let $h : \mathbb{R} \rightarrow \mathbb{R}_+$ be a function defined by

$$h(y|z) := \frac{1}{2}(y - z)^2 + \frac{\lambda}{L}|y|.$$

Observe that

$$\begin{aligned} & \frac{L}{2} \|\mathbf{W}^* - \mathbf{W}_{k+\frac{1}{3}}^*\|_F^2 + \lambda \sum_{i=1}^m \|\mathbf{W}_{i,:}^*\|_1 \\ &= L \sum_{i,j} h(\mathbf{W}_{ij}^* | \mathbf{W}_{k+\frac{1}{3},ij}^*). \end{aligned}$$

Hence problem Equation 9 can be split into $m \times n$ independent subproblems of dimension 1 and we only need to focus on solving each one of them. Note that h is convex but not smooth. It suffices to find a point $\mathbf{W}_{k+\frac{2}{3},ij}^*$ such that

$$0 \in \partial h(\mathbf{W}_{k+\frac{2}{3},ij}^* | \mathbf{W}_{k+\frac{1}{3},ij}^*),$$

where ∂ denotes the sub-differential operator. Observe that

$$\partial h(y|z) = \begin{cases} y - z + \frac{\lambda}{L}, & \text{if } y > 0, \\ y - z - \frac{\lambda}{L}, & \text{if } y < 0, \\ \{y - z + u\frac{\lambda}{L} \mid u \in [-1, 1]\}, & \text{if } y = 0. \end{cases}$$

We now solve for $0 \in \partial h(y|z)$ by considering the following cases:

- If $y > 0$, then we set $y - z + \frac{\lambda}{L} = 0$. This gives $y = z - \frac{\lambda}{L}$ and requires $z > \frac{\lambda}{L}$.
- If $y < 0$, then we set $y - z - \frac{\lambda}{L} = 0$. This gives $y = z + \frac{\lambda}{L}$ and requires $z < -\frac{\lambda}{L}$.
- If $y = 0$, then we want $0 \in \{y - z + u\frac{\lambda}{L} \mid u \in [-1, 1]\}$. This requires $-\frac{\lambda}{L} < z < \frac{\lambda}{L}$.

Hence, $0 \in \partial h(\mathbf{W}_{k+\frac{2}{3},ij}^* \mid \mathbf{W}_{k+\frac{1}{3},ij}^*)$ yields

$$\mathbf{W}_{k+\frac{2}{3},ij}^* = \begin{cases} \mathbf{W}_{k+\frac{1}{3},ij}^* - \frac{\lambda}{L}, & \text{if } \mathbf{W}_{k+\frac{1}{3},ij}^* > \frac{\lambda}{L}, \\ \mathbf{W}_{k+\frac{1}{3},ij}^* + \frac{\lambda}{L}, & \text{if } \mathbf{W}_{k+\frac{1}{3},ij}^* < -\frac{\lambda}{L}, \\ 0, & \text{otherwise,} \end{cases}$$

which is given by $\text{SoftShrinkage}_{\lambda/L}(\mathbf{W}_{k+\frac{1}{3},ij}^*)$.

Finally, according to (Beck and Teboulle, 2009), we add a Nesterov acceleration step by setting $t_0 = 1$ and computing

$$t_{k+1} = \frac{1}{2} \left(1 + \sqrt{1 + 4t_k^2} \right), \quad (10)$$

$$\mathbf{W}_{k+1}^* = \mathbf{W}_{k+\frac{2}{3}}^* + \frac{t_k - 1}{t_{k+1}} (\mathbf{W}_{k+\frac{2}{3}}^* - \mathbf{W}_k^*), \quad (11)$$

which gives steps Equation 4c and Equation 4d.

The above illustrates the details of the FISTA iterations.

C Novelty Compared to Traditional LASSO-based Pruning

Compared to traditional LASSO-based or ℓ_1 -regularization pruning, our work introduces several key innovations that advance the state-of-the-art in post-training pruning for LLMs.

We develop a LASSO-based, layer-wise pruning approach where each linear layer is optimized independently through a convex formulation (equation 3). This contrasts with (Wen et al., 2016), which incorporates group LASSO regularization into the training loss, resulting in a non-convex objective that may converge to suboptimal solutions.

Our convex formulation guarantees stable convergence while maintaining computational tractability.

While (He et al., 2017) adapts LASSO for channel pruning in CNNs using heuristic alternating optimization, we employ FISTA with provable $O(1/k^2)$ convergence. Our implementation leverages closed-form solutions involving only matrix-matrix multiplications and element-wise operations, enabling efficient GPU acceleration, which is a critical advantage when scaling to billion-parameter LLMs where previous methods become computationally prohibitive.

We introduce a bisection-based method to automatically determine the optimal sparsity-controlling parameter λ for any target sparsity level. This represents a significant improvement over (He et al., 2017)'s linear incremental strategy, offering both faster convergence and more reliable results through principled interval halving.

The framework natively supports both unstructured sparsity and hardware-friendly 2:4 semi-structured patterns, enabling practical deployment on modern accelerators like NVIDIA Ampere GPUs (Bai and Li, 2023). This hardware compatibility was not addressed in prior LASSO-based pruning methods.

A novel error correction mechanism specifically designed for transformer architectures compensates for pruning-induced perturbations within each layer. Comprehensive ablation studies demonstrate its effectiveness in maintaining model accuracy compared to baseline approaches.

While previous works have explored individual components of LASSO-based pruning, our method represents the first unified framework that simultaneously addresses all these aspects for modern LLMs.

D Proof of Theorem 1

Assume the weight matrix has p parameters. The sparsity function $s(\lambda)$ is non-decreasing and piecewise-constant with at most $p + 1$ plateaus, as established by the piecewise-linear structure of ℓ_1 -regularized solution paths. Assume the smallest plateau has length L . The bisection algorithm iteratively maintains an interval $[\lambda_l^{(k)}, \lambda_r^{(k)}]$ at step k , where $\lambda_l^{(k)}$ and $\lambda_r^{(k)}$ denote the lower and upper bounds respectively, preserving the invariant $s(\lambda_l^{(k)}) \leq s \leq s(\lambda_r^{(k)})$. At each iteration, the midpoint $\lambda_m = (\lambda_l^{(k)} + \lambda_r^{(k)})/2$ is computed. The interval is updated by setting $\lambda_l^{(k+1)} \leftarrow \lambda_m$ if

$s(\lambda_m) < s$, or $\lambda_r^{(k+1)} \leftarrow \lambda_m$ otherwise. This procedure preserves the invariant while halving the interval width $\delta_k = \lambda_r^{(k)} - \lambda_l^{(k)}$ at every step.

As the iterations proceed, within $k = O(\log \frac{\delta_0}{L})$ steps, we must have $\delta_k \leq L$. By the definition of L , for all $\lambda \in [\lambda_l^{(k)}, \lambda_r^{(k)}]$, there are at most two possible values of $s(\lambda)$. Therefore, one of the endpoints, $\lambda_l^{(k)}$ or $\lambda_r^{(k)}$ must be the desired λ such that $s(\lambda) = s$, and the algorithm should have already terminated.

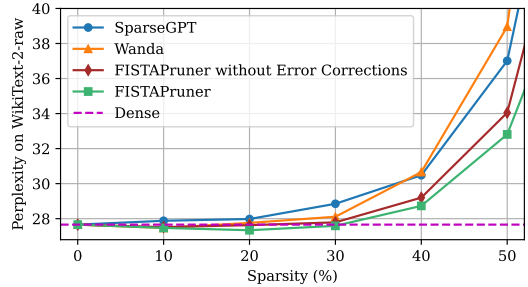
E Additional Results

E.1 Perplexity Results on PTB

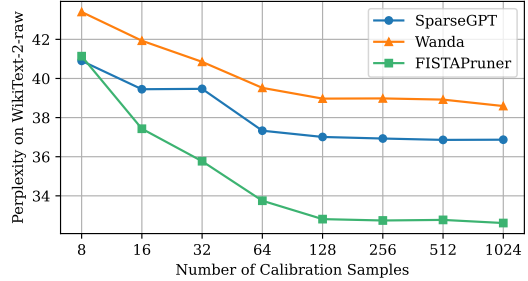
We present the PTB perplexity results of pruned OPT, LLaMA, LLaMA-2, LLaMA-3, and Qwen2.5 models under 50% unstructured and 2:4 semi-structured sparsity in Tables 6 and 7. FISTAPruner outperforms baseline methods on all OPT, LLaMA and LLaMA-3 models, as well as on most LLaMA-2 models on the PTB dataset. The sole exception is the pruning of the LLaMA-2-70B model under 50% unstructured sparsity, where FISTAPruner surpasses Wanda but falls short of SparseGPT. This underperformance may be due to the generally poorer performance of LLaMA-2 models compared to similarly sized models from other families. For instance, the dense LLaMA-2-13B model exhibits a PTB perplexity of 56.52, even higher than the smaller LLaMA-2-7B model, which has a perplexity of 50.19. Moreover, we observe that the PTB perplexity results for all dense LLaMA and LLaMA-2 models are consistently higher than those for similarly sized OPT models; for example, the LLaMA-2-13B’s perplexity of 56.52 far exceeds the smallest OPT-125M model’s 38.99. In contrast, LLaMA-3 models show significantly better performance on the PTB dataset. Besides, FISTAPruner performs consistently better than baselines on Qwen models.

E.2 Perplexity Results on C4

The C4 perplexity results of pruned OPT, LLaMA, LLaMA-2, LLaMA-3, and Qwen2.5 models under 50% unstructured and 2:4 semi-structured sparsity are shown in Tables 6 and 7. FISTAPruner performs consistently better than the baselines.

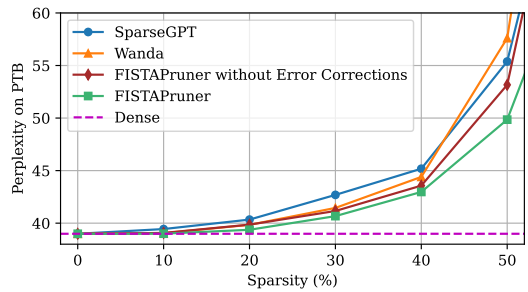


(a) Intra-layer error corrections ablation.

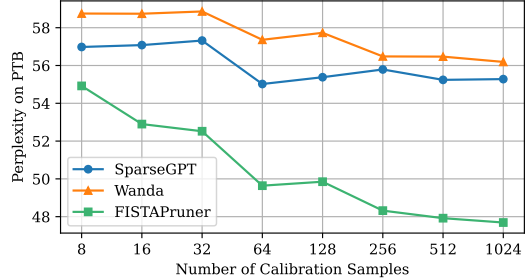


(b) Calibration samples ablation.

Figure 4: Studies of FISTAPruner on the WikiText dataset on OPT-2 125M, showcasing the effects of intra-layer error correction and varying calibration sample sizes.



(a) Intra-layer error corrections ablation.



(b) Calibration samples ablation.

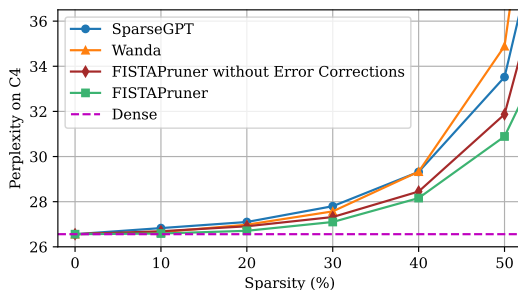
Figure 5: Studies of FISTAPruner on the PTB dataset on OPT-125M, showcasing the effects of intra-layer error correction and varying calibration sample sizes.

Table 6: PTB perplexity of pruned OPT models under 50% unstructured and 2:4 semi-structured sparsity. FISTAPruner outperforms baseline methods.

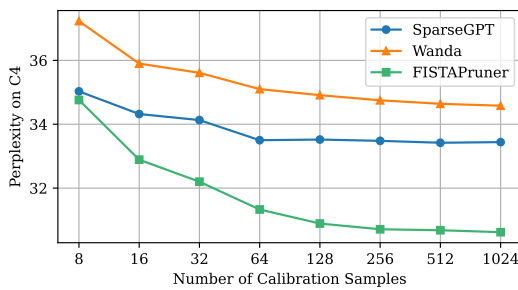
OPT								
Method	Sparsity	125M	350M	1.3B	2.7B	6.7B	13B	30B
Dense	0%	38.99	31.07	20.29	17.97	15.77	14.52	14.04
SparseGPT	50%	55.38	43.58	25.64	20.52	17.38	15.98	14.97
Wanda	50%	57.60	55.47	27.98	21.85	17.92	17.45	15.47
FISTAPruner	50%	49.79	41.26	25.08	20.15	17.08	15.87	14.92
SparseGPT	2:4	94.21	72.82	37.30	26.87	21.65	18.69	16.56
Wanda	2:4	111.55	135.98	43.85	34.64	25.07	22.16	21.65
FISTAPruner	2:4	67.80	59.51	36.26	24.43	20.04	18.08	16.18

Table 7: PTB perplexity (\downarrow) of pruned LLaMA, LLaMA-2, LLaMA-3, and Qwen2.5 models under 50% unstructured and 2:4 semi-structured sparsity.

Method	Sparsity	LLaMA				LLaMA-2			LLaMA-3		Qwen2.5	
		7B	13B	30B	65B	7B	13B	70B	8B	70B	0.5B	1.5B
Dense	0%	41.15	28.10	23.51	25.07	50.19	56.52	22.68	10.17	7.87	26.03	17.85
SparseGPT	50%	79.67	37.49	26.14	27.64	1020.01	95.41	24.87	14.00	9.24	38.41	24.89
Wanda	50%	80.48	36.43	26.64	25.77	97.58	86.79	26.07	15.54	9.44	46.83	27.15
FISTAPruner	50%	58.67	35.30	25.63	25.15	96.72	78.23	25.36	12.93	8.88	41.62	23.15
SparseGPT	2:4	154.62	71.68	32.44	32.91	1163.57	154.15	31.51	23.42	13.01	75.98	41.45
Wanda	2:4	211.40	74.29	35.56	33.39	587.54	224.55	33.97	48.96	14.17	142.19	103.61
FISTAPruner	2:4	91.84	64.04	30.86	30.78	361.16	136.84	31.49	22.60	11.11	57.34	35.20



(a) Intra-layer error corrections ablation.



(b) Calibration samples ablation.

Figure 6: Studies of FISTAPruner on the C4 dataset on OPT-125M, showcasing the effects of intra-layer error correction and varying calibration sample sizes.

F Ablation Studies

F.1 Intra-layer Error Corrections

We perform ablation studies on the OPT-125M model with 50% unstructured sparsity to evaluate the intra-layer error correction mechanism. We compare the performance of FISTAPruner with and without the intra-layer error correction mechanism, with perplexity results on the WikiText, PTB and C4 datasets displayed in Figures 4(a), 5(a), and 6(a). We observe that the perplexity of the pruned model incorporating this mechanism consistently outperforms the version without it, thereby confirming its effectiveness. Moreover, FISTAPruner, even without the intra-layer error correction mechanism, outperforms existing methods such as SparseGPT and Wanda. This underscores the effectiveness of applying convex optimization theory and algorithms to pruning problems. Additionally, we treat each decoder layer as an independent pruning unit with intra-layer error correction, rather than using both intra- and inter-layer error correction for a global mechanism, for the following reasons: (1) Intra-layer error correction allows independent pruning of each decoder layer, enabling distribution of the task across multiple devices and improving overall efficiency. (2) While combining intra- and inter-layer error correction can reduce error accumulation, it is effective only at low sparsity levels. At higher sparsity, global error correction domi-

Table 8: C4 perplexity (\downarrow) of pruned OPT models under 50% unstructured and 2:4 semi-structured sparsity. FISTAPruner outperforms baseline methods.

Method	Sparsity	OPT							
		125M	350M	1.3B	2.7B	6.7B	13B	30B	
Dense	0%	26.56	22.59	16.07	14.34	12.71	12.06	11.45	
SparseGPT	50%	33.52	29.14	19.23	15.77	13.73	12.98	11.96	
Wanda	50%	34.89	34.46	20.63	16.44	14.25	13.57	12.32	
FISTAPruner	50%	30.93	27.36	18.56	15.58	13.61	12.94	11.92	
SparseGPT	2:4	52.11	46.36	25.77	19.35	16.44	14.85	13.18	
Wanda	2:4	64.73	88.62	28.59	22.88	19.00	16.19	16.18	
FISTAPruner	2:4	38.08	36.45	24.29	17.82	15.35	14.19	12.78	

Table 9: C4 perplexity (\downarrow) of pruned LLaMA, LLaMA-2, LLaMA-3, and Qwen2.5 models under 50% unstructured and 2:4 semi-structured sparsity. FISTAPruner outperforms baseline methods.

Method	Sparsity	LLaMA				LLaMA-2			LLaMA-3		Qwen2.5	
		7B	13B	30B	65B	7B	13B	70B	8B	70B	0.5B	1.5B
Dense	0%	7.34	6.80	6.13	5.81	7.04	6.52	5.53	9.01	6.82	20.39	15.13
SparseGPT	50%	9.33	8.14	7.34	6.66	9.00	7.96	6.25	13.93	9.34	28.60	19.83
Wanda	50%	9.34	8.15	7.29	6.71	8.94	8.04	6.30	14.97	9.80	35.36	21.69
FISTAPruner	50%	8.90	7.96	7.05	6.49	8.62	7.73	6.22	13.12	8.94	27.29	18.89
SparseGPT	2:4	13.65	11.38	9.50	8.41	13.58	11.39	7.99	24.16	14.81	49.72	31.85
Wanda	2:4	14.47	12.11	9.46	8.78	15.07	12.13	7.89	36.70	14.47	131.21	66.58
FISTAPruner	2:4	11.95	10.27	8.81	7.82	12.41	10.34	7.59	23.15	12.18	40.66	27.00

nates layer-specific pruning, leading to worse performance. A detailed analysis of this is provided in Appendix G.

F.2 Calibration Data and Warm Start

We conduct studies to evaluate the impact of the number of calibration samples and warm start.

Amount of Calibration Data. We investigate the performance of FISTAPruner and existing methods, SparseGPT and Wanda, in relation to the number of calibration data samples, which we vary in powers of two. The results for the WikiText dataset with the OPT-125M model at 50% sparsity are shown in Figure 4(b). We observe that using more calibration samples significantly enhances performance, but only up to a certain point as the improvement curve quickly flattens. This finding aligns with observations in (Frantar and Alistarh, 2023; Sun et al., 2023). Given that using more samples increases computational and memory costs, we consistently use 128 calibration samples in all our experiments. The results of pruning performance in relation to the number of calibration data samples on PTB and C4 datasets are displayed in Figures 5(b) and 6(b). The same curve pattern as shown in Figure 4(b) is observed.

Choice of Calibration Dataset. We evaluate perplexity across different calibration datasets on

OPT-125M. The C4 calibration dataset consistently achieved the lowest total perplexity scores (113.59 at 50% sparsity, 155.47 at 2:4 sparsity), outperforming both WikiText and PTB. This aligns with findings from recent work (Ji et al., 2024), demonstrating that web-scale, diverse datasets like C4 tend to produce more robust pruning results compared to domain-specific calibration data. Three factors likely contribute to C4’s superior performance: (1) Its broad domain coverage better represents the model’s pretraining distribution, (2) The dataset’s size and diversity provide more stable importance score estimation during pruning, and (3) Reduced domain mismatch between calibration and test conditions. The performance gap becomes more pronounced with stricter sparsity constraints (2:4 vs 50%), underscoring how calibration data quality grows increasingly critical with aggressive pruning.

Warm Start. Warm-starting is a widely recognized technique in optimization that leverages starting at a point near the optimal solution to significantly reduce the total convergence time. In our framework, we evaluate the efficiency of warm start mechanism as follows: Dense Weights $<$ Magnitude Pruning \approx Wanda $<$ SparseGPT. Dense weights, though readily obtainable, slow down the convergence due to their significant deviation from the target spar-

Table 10: Perplexity across calibration datasets and sparsity levels of pruned OPT-125M.

Dataset	Sparsity	WikiText	C4	PTB	Total
WikiText	50%	30.74	35.03	50.48	116.26
C4	50%	32.82	30.90	49.87	113.59
PTB	50%	40.07	40.81	41.71	122.59
WikiText	2:4	37.22	47.85	72.39	157.45
C4	2:4	45.69	39.21	70.57	155.47
PTB	2:4	61.18	63.59	46.96	171.74

sity level. Magnitude pruning, involving absolute value computations and comparisons, meets sparsity requirements but generally yields lower-quality solutions. Wanda, requiring absolute value computations, ℓ_2 -norm calculations of activation columns, and element-wise multiplication, is nearly as efficient as magnitude pruning. This near parity in efficiency is due to our model’s reliance on activation data from calibration, allowing ℓ_2 -norm computations to occur incidentally during the process. Despite their similar efficiencies, Wanda’s solutions markedly outperform those from magnitude pruning. SparseGPT is less efficient compared with magnitude pruning and Wanda but may provide a stronger initial point.

To further illustrate the impact of warm start on FISTAPruner, we conduct additional tests using both dense weights and magnitude pruning results as starting points. The results are presented in Table 11, which indicates that FISTAPruner still can achieve comparable results.

G Why Intra-Layer Error Correction Is Preferred Over Intra- and Inter-Layer Error Correction

We apply only the intra-layer error correction mechanism for two reasons:

1. **Parallelization:** Intra-layer error correction enables independent pruning of each decoder layer, allowing us to distribute the pruning task across multiple devices by assigning different decoder layers to different devices. This increases the overall pruning efficiency.
2. **Sparsity Sensitivity:** While combining intra- and inter-layer error correction could intuitively reduce error accumulation across the network, we found that this approach is effective only at low sparsity levels. When the pruning task becomes harder (i.e., higher sparsity), global error correction tends to overshadow

the pruning process of individual layers, ultimately leading to worse performance.

The first reason is straightforward; we will explain the second reason in more detail below.

We conducted a series of comparison experiments on OPT-125M at sparsity levels of 5%, 10%, 20%, and 50%. The experiments included three conditions: intra-layer error correction only, both intra- and inter-layer error correction, and no error correction. The results are presented in the following tables.

As shown in the results above, we summarize the perplexity comparison across different sparsity levels as follows:

- **5% and 10%:** intra- and inter-layer error correction < intra-layer error correction only < no error correction.
- **20%:** intra-layer error correction only < intra- and inter-layer error correction < no error correction.
- **50%:** intra-layer error correction only < no error correction < intra- and inter-layer error correction.

First, the results confirm the effectiveness of our intra-layer error correction mechanism, as it consistently outperforms the no-error-correction approach.

Second, the results confirm the effectiveness of using both intra- and inter-layer error correction at low sparsity levels, as it consistently outperforms the intra-layer error correction alone at 5% and 10% sparsity.

Third, the results show that using both intra- and inter-layer error correction is sensitive to sparsity levels and tends to perform worse at higher sparsity. Specifically, at 20% sparsity, it underperforms compared to intra-layer error correction alone, and at 50% sparsity, it even performs worse than the no-error-correction approach.

To explain why the use of both intra- and inter-layer error correction is sensitive to sparsity levels, we believe this occurs because higher sparsity levels make the pruning task more difficult, leading to greater error accumulation across layers. When both intra- and inter-layer error correction are applied, mitigating the accumulated error from previous layers may dominate the optimization objective in deeper layers, causing the pruning performance of the current layer to suffer.

Table 11: Perplexity (\downarrow) results for WikiText, PTB and C4 under 50% unstructured and 2:4 semi-structured sparsity. FISTAPruner is initialized with magnitude pruning and dense weights.

Method	Sparsity	WikiText	PTB	C4
Magnitude	25%	31.38	38.99	26.56
FISTAPruner (initialized with magnitude pruning)	25%	28.67	40.29	27.07
FISTAPruner (initialized with dense weights)	25%	28.66	40.27	27.07
Magnitude	50%	193.35	276.17	141.00
FISTAPruner (initialized with magnitude pruning)	50%	<u>38.62</u>	52.26	32.87
FISTAPruner (initialized with dense weights)	50%	<u>38.62</u>	<u>52.43</u>	<u>32.89</u>
Magnitude	2:4	343.91	810.42	223.98
FISTAPruner (initialized with magnitude pruning)	2:4	57.43	78.37	45.20
FISTAPruner (initialized with dense weights)	2:4	<u>58.55</u>	<u>80.72</u>	<u>45.51</u>

Table 12: OPT-125M under 5% Sparsity

	WikiText	C4	PTB
Intra-layer Error Correction Only	27.64	26.57	38.99
Intra-layer and Inter-layer Error Correction	27.63	26.56	38.98
No Error Correction	27.69	26.60	38.98

Table 13: OPT-125M under 10% Sparsity

	WikiText	C4	PTB
Intra-layer Error Correction Only	27.47	26.59	39.00
Intra-layer and Inter-layer Error Correction	27.43	26.58	39.04
No Error Correction	27.52	26.69	39.07

Table 14: OPT-125M under 20% Sparsity

	WikiText	C4	PTB
Intra-layer Error Correction Only	27.36	26.71	39.39
Intra-layer and Inter-layer Error Correction	27.37	26.72	39.53
No Error Correction	27.61	26.91	39.85

Table 15: OPT-125M under 50% Sparsity

	WikiText	C4	PTB
Intra-layer Error Correction Only	33.54	30.93	49.79
Intra-layer and Inter-layer Error Correction	35.90	32.93	55.24
No Error Correction	34.48	32.24	54.11

Mathematically, let \mathbf{W}_k and \mathbf{X}_k represent the weight matrix and the activation of the k -th layer in the original network, respectively. Similarly, let \mathbf{W}_k^* and \mathbf{X}_k^* denote the pruned weight matrix and the corresponding activation in the pruned network. In a layer-wise pruning scheme with both intra- and inter-layer error correction mechanisms, we minimize the loss for each layer individually:

$$\|\mathbf{W}_k^* \mathbf{X}_k^* - \mathbf{W}_k \mathbf{X}_k\|_F^2. \quad (12)$$

\mathbf{X}_k depends on the activation from the previous

layer:

$$\mathbf{X}_k = f_k(\mathbf{W}_{k-1} \mathbf{X}_{k-1}), \quad (13)$$

where f_k represents some operations (e.g., activation function or normalization). Therefore, we can express the pruned activations recursively as:

$$\mathbf{X}_k^* = f_k(\mathbf{W}_{k-1}^* \mathbf{X}_{k-1}^*). \quad (14)$$

The error at layer k is defined as:

$$\Delta \mathbf{X}_k = f_k(\mathbf{W}_{k-1}^* \mathbf{X}_{k-1}^*) - f_k(\mathbf{W}_{k-1} \mathbf{X}_{k-1}). \quad (15)$$

Under high sparsity levels, this amplification often results in the accumulated error $\Delta \mathbf{X}_k$ becoming dominant at deeper layers. Thus, for large k , considering both intra- and inter-layer error correction mechanisms, we have:

$$\|\mathbf{W}_k^*(\mathbf{X}_k + \Delta \mathbf{X}_k) - \mathbf{W}_k \mathbf{X}_k\|_F^2 \quad (16)$$

$$\approx \|\mathbf{W}_k^* \Delta \mathbf{X}_k - \mathbf{W}_k \mathbf{X}_k\|_F^2. \quad (17)$$

As a result, the optimization process shifts focus towards correcting this accumulated error rather than pruning the current weight matrix \mathbf{W}_k .

In other words, minimizing the term in Equation 16 primarily addresses the error correction from previous layers rather than properly pruning the weight matrix \mathbf{W}_k , which negatively impacts the pruning performance in deeper layers.

H Inference Efficiency of Pruned Models

FISTAPruner supports both unstructured and 2:4 semi-structured sparsity patterns while maintaining model accuracy and compatibility with standard inference kernels. Although our primary focus is on optimizing post-pruning accuracy rather than inference acceleration, the sparsity patterns generated by FISTAPruner align with those evaluated in prior work, enabling direct comparisons of inference efficiency.

For unstructured sparsity, prior studies have demonstrated practical speedups on CPU platforms. For instance, DeepSparse achieves a $1.82 \times$ end-to-end speedup for OPT-2.7B at 50% sparsity (Frantar and Alistarh, 2023). However, unstructured sparsity currently offers limited acceleration on GPUs due to hardware constraints. In contrast, 2:4 semi-structured sparsity is natively supported on modern NVIDIA Ampere GPUs (Bai and Li, 2023). Empirical results show that this format yields up to $1.5 \times$ speedup for LLaMA-2-7B and LLaMA-2-13B models during inference (Ashkboos et al., 2024).

Since FISTAPruner produces models with identical sparsity formats to those studied in (Frantar and Alistarh, 2023; Ashkboos et al., 2024), we expect similar inference speedups in practice. This compatibility ensures that our pruning framework remains practical for deployment while achieving its primary goal of high-accuracy sparse models.

I Usage of LLMs

LLMs have been utilized during the preparation of this work to assist with proofreading, grammar correction, and enhancing the clarity and fluency of the paper.